Theory of strong intrinsic mixing of particle suspensions in vortex magnetic fields

James E. Martin
Sandia National Laboratories, Albuquerque, New Mexico 87185-1421, USA
(Received 12 February 2008; revised manuscript received 24 September 2008; published 27 January 2009)

Recent experiments have shown that a type of triaxial magnetic field we call a vortex field can induce strong mixing in a magnetic particle suspension. A vortex triaxial field consists of a rotating magnetic field in a horizontal plane, with a dc field applied normal to this. The mixing torque is found to be independent of the field frequency and fluid viscosity over a broad range; scales as the square of the applied field; and is strongest for a balanced triaxial field—one in which the root-mean-square amplitudes of the three field components are equal. In this paper we show that these anomalous effects are consistent with the formation of volatile particle chains that have a precessionlike motion. Theoretical results are given for both particle chains and magnetic rods for arbitrary vortex field angles. A key conclusion is that the mixing torque is independent of particle size, making this mixing technique scale adaptive, and thus suitable for microfluidics applications.

DOI: 10.1103/PhysRevE.79.011503 PACS number(s): 83.80.Gv, 75.50.Tt, 75.60.Ej, 81.05.Qk

INTRODUCTION

Fluid mixing is a sufficiently important problem that countless methods have been devised to accomplish this task. Yet none of these methods have proven highly successful in microcavities and channels, because the small size scale makes the engineering and fabrication of conventional mixing devices difficult. Even simple mixing cells fail on the microscale, because it is difficult to create flow rates large enough to introduce nonlaminar flow. In this paper we discuss the microscopic mechanism of a method of mixing that is scale adaptive and that creates homogeneous mixing even in irregular cavities. This method is based on the application of a "vortex" magnetic field to a suspension of magnetically soft particles.

This technique opens the possibility of introducing magnetic nanoparticles into microchannels to create strong fluid mixing. These particles could be confined magnetically, or by the use of barriers such as pillars. A vortex field can be created by compact, open-air Helmholtz coils, since only modest fields ($\sim$0.01 T) are required. For these reasons we believe vortex magnetic field mixing could become a viable technology for microfluidics devices and other challenging mixing problems.

A vortex magnetic field is a particular example of a triaxial magnetic field. Recent experiments [1,2] have shown that a variety of dynamical phenomena can be induced by subjecting suspensions of magnetic particles to triaxial magnetic fields. A triaxial field is composed of three orthogonal field components, at least two of which are alternating. (In our laboratory these field components are produced by Helmholtz coils in series resonance with tunable capacitor banks. Component frequencies as large as 2500 Hz are possible, with induction field amplitudes ranging up to 0.05 T.) A *vortex* triaxial field is of special interest because it creates a body torque that results in strong mixing throughout the volume of a particle suspension. A vortex field can be viewed as the sum of two fields: a purely rotating field, which we take to lie in the x-y plane, and a dc field applied normal to the plane of rotation, that is, parallel to the z axis (see Fig. 1). The vortex field has three parameters: frequency f, magnitude H_0, and polar field angle θ_f. These parameters are defined through

$$\mathbf{H}_0 = H_0\{\sin\theta_f[\sin(2\pi ft)\hat{\mathbf{x}} + \cos(2\pi f)\hat{\mathbf{y}}] + \cos\theta_f\hat{\mathbf{z}}\},$$

where the dc field direction (z axis) is the mixing axis. For a balanced vortex field the three rms field components are equal, so the vortex field angle is given by $\sin\theta_f = \sqrt{2/3}$, $\cos\theta_f = \sqrt{1/3}$, and $\theta_f \approx 54.7°$.

The goal of this paper is to understand the cause of the unusual mixing behavior we have observed for suspensions of Fe particles [3], which is contrary in all regards to the behavior of mixing with single magnetic bodies, such as stir bars. In the field regime where mixing occurs the observed anomalies include the following. (1) The mixing torque is independent of field frequency. For stir bar mixing the torque is proportional to frequency. (2) The torque is independent of the fluid viscosity, whereas with a stir bar the torque is proportional to viscosity. (3) The torque increases quadratically with the field magnitude, whereas the torque is independent of the field for a stir bar. (4) With a stir bar a rotating field is optimal for mixing, whereas for particle suspensions a vortex field is necessary.

These observations have led us to postulate that vortex mixing is due to the formation of particle chains that follow

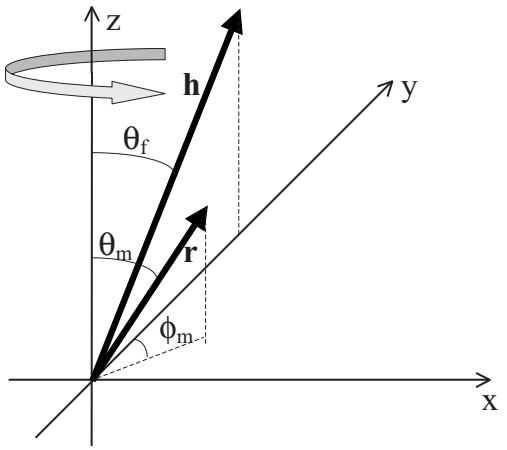

FIG. 1. The coordinate system, showing both the chain and field vectors. The field is rotating in the direction of $-\phi$. When the projection of the field vector onto the x-y plane is parallel to the y axis, the azimuthal angle ϕ_m of the chain is its phase lag.

the vortex field with a precessionlike motion, each acting like a miniature stir bar. In developing this postulate we will show that the anomalies cited above are due to the adaptive nature of these chains, whose length changes in response to alterations in the field strength and frequency, as well as the fluid viscosity.

The calculation of chains "precessing" with a vortex field sounds like a standard phase lag problem, but there is an interesting aspect to it: the polar angle of the chain decreases from the vortex field angle to 0° as the phase lag of the chain behind the field increases from 0° to 90°. In this paper we consider the stationary orbits for particle chains as functions of field amplitude and frequency, liquid viscosity, chain length and radius, and particle susceptibility. We develop stability criteria for these orbits to develop an expression for the magnetic mixing torque density of particle suspensions. We find that these expressions account for the experimental observations described above.

Analogous calculations are performed for dilute suspensions of unagglomerated rods, to illustrate the difference between a fixed magnetic structure and volatile particle chains that can fragment and aggregate. For example, it is shown that for dilute rods the torque increases with field frequency, and has a complex and weak dependence on the field amplitude that is highly dependent on the vortex field angle.

Our approach to vortex field mixing is based on earlier single-chain calculations for the shear-thinning viscosity of electrorheological fluids [4]. This single-chain approach has already been adapted to the study of single-chain dynamics in a rotating magnetic field [5]. In the case of particle suspensions subjected to steady shear in a constant magnetic or electric field, it is known that the particles can form sheetlike structures [6–10] that make a chain interpretation problematic at high particle concentrations. Likewise, particles tend to form sheets in a rotating field, due to the time-average negative dipolar interactions induced by the field [11]. In a balanced vortex field average particle interactions are weak [1], so we expect a chain theory to be a valid here.

Finally, a few general comments about the approach we take. To simplify the analysis we model a chain of particles in a vortex field as a linear structure. A real particle chain will have a sigmoidal shape, and for the case of a chain of dipoles subjected to shear flow normal to the field (i.e., the case of magneto- or electrorheology) we have given an expression for this shape [4]. However, we have also shown that a proper accounting of this shape has little effect on the expression for the fluid rheology. The computation of the mixing torque in a vortex field is a related problem, and the effect of chain shape is expected to be small compared to the other approximations we make to obtain an expression for the mixing torque. We also point out that, although this paper is written in the language of magnetism, the same effects can be produced with vortex electric fields and suspensions of dielectric particles, although, because it is more difficult to produce a uniform vortex electric field, future experimental work will probably focus on magnetic systems.

MAGNETIC MIXING OF PARTICLE SUSPENSIONS

Force between dipoles

We start by developing an expression for the force between dipoles. We will compute the interaction force on a dipole labeled 2 due to the presence of a nearby dipole labeled 1. Dipole 1 is located at the origin and dipole 2 is located at the point $\mathbf{r}$. The magnetic field $\mathbf{H}_1$ at point $\mathbf{r}$ due to a point dipole $\mathbf{m}_1$ located at the origin is [12]

$$\mathbf{H}_1 = \frac{1}{4\pi r^3}[3(\mathbf{m}_1 \cdot \hat{\mathbf{r}})\hat{\mathbf{r}} - \mathbf{m}_1], \tag{1}$$

where $\hat{\mathbf{r}}$ is a unit vector that points from dipole 1 to dipole 2. The gradient of this field creates a force $\mathbf{F}_2 = \mu_0 \mathbf{m}_2 \cdot \nabla \mathbf{H}_1$ on the second dipole of moment $\mathbf{m}_2$, where $\mu_0 = 4\pi \times 10^{-7}$ H/m is the vacuum permeability [12]. For static fields this force expression is equivalent to

$$\mathbf{F}_2 = \mu_0 \nabla (\mathbf{m}_2 \cdot \mathbf{H}_1). \tag{2}$$

Taking derivatives gives the Cartesian components of the force on dipole 2,

$$c^{-1}F_{2,w} = -\frac{w}{r}[5(\mathbf{m}_1 \cdot \hat{\mathbf{r}})(\mathbf{m}_2 \cdot \hat{\mathbf{r}}) - \mathbf{m}_1 \cdot \mathbf{m}_2] + (\mathbf{m}_1 \cdot \hat{\mathbf{w}})(\mathbf{m}_2 \cdot \hat{\mathbf{r}}) + (\mathbf{m}_1 \cdot \hat{\mathbf{r}})(\mathbf{m}_2 \cdot \hat{\mathbf{w}}), \tag{3}$$

where $c = 3\mu_0/(4\pi r^4)$ and w denotes x, y, or z. In the case where the dipole moments are equal the force simplifies to

$$f_c^{-1}F_w = -\frac{w}{r}\left[5\frac{(\mathbf{m} \cdot \hat{\mathbf{r}})^2}{m^2} - 1\right] + 2\frac{m_w(\mathbf{m} \cdot \hat{\mathbf{r}})}{m^2}, \tag{4}$$

where we have now dropped the subscript 2 with the understanding that this is the force on dipole 2, and $f_c = (3\mu_0/4\pi r^4)m^2$. In the special case where the dipole moments are aligned along the z axis it is easily shown that

$$\mathbf{F} = -f_c[(3\cos^2\theta - 1)\hat{\mathbf{r}} - \sin 2\theta\, \hat{\boldsymbol{\theta}}], \tag{5}$$

where θ is the angle of $\mathbf{r}$ to the z axis.

Force between enchained particles

To compute the force between particles in a chain we will make the simplifying approximation that the dipoles are induced by the field alone. This fixed point dipole approximation is exact only when the applied field is more than sufficiently strong to saturate the particle moments. We will later consider the effect of the dipole fields on the induced moments, which is important at low applied fields. We will not consider the effect of multipolar interactions, which although of consequence in nonsaturating fields, would make this theory very complex.

If the dipoles are induced by the applied field alone the moment can be written $\mathbf{m} = m\hat{\mathbf{h}}$, where $\hat{\mathbf{h}} = (0, H_y, H_z)/H = (0, \sin\theta_f, \cos\theta_f)$ is a unit vector along the applied field $\mathbf{H}$, which we take to be in the y-z plane (Fig. 1). In terms of the spherical angles defined in Fig. 1—the polar angle θ and the azimuthal phase lag angle ϕ—the unit vector along the chain of particles is $\hat{\mathbf{r}} = (\sin\phi_m \sin\theta_m, \cos\phi_m \sin\theta_m, \cos\theta_m)$. The force components can now be written

$$f_c^{-1}F_w = -\frac{w}{r}[5(\hat{\mathbf{h}}\cdot\hat{\mathbf{r}})^2 - 1] + 2\frac{m_w}{m}(\hat{\mathbf{h}}\cdot\hat{\mathbf{r}}), \tag{6}$$

where $\hat{\mathbf{h}}\cdot\hat{\mathbf{r}}=\cos\alpha$ and α is the angle between the chain axis and the applied field. In terms of the spherical coordinates,

$$\cos\alpha = \sin\theta_f\cos\phi_m\sin\theta_m + \cos\theta_f\cos\theta_m. \tag{7}$$

Finally, we note that $m_x/m=0$, $m_y/m=\sin\theta_f$, and $m_z/m=\cos\theta_f$.

Stationary particle orbits

In a typical problem involving a phase lag—for example, a particle chain driven by a purely rotating field—the orbit is determined by the phase lag ϕ alone. However, for a vortex field the polar angle is also an important variable. For a stationary orbit the polar angle θ_m of a chain will generally be smaller than the vortex field angle θ_f and will depend in some way on the phase lag ϕ_m. In the following we compute a closure relation between these three angles for chains in stationary orbits.

It is helpful to express the particle forces in spherical coordinates, $\mathbf{F}=F_r\hat{\mathbf{r}}+F_\theta\hat{\boldsymbol{\theta}}+F_\phi\hat{\boldsymbol{\phi}}$. We first consider the polar force $F_\theta=\mathbf{F}\cdot\hat{\boldsymbol{\theta}}$, since this force determines the stationary chain orbits. In Cartesian coordinates the polar angle is $\hat{\boldsymbol{\theta}}=\sin\phi_m\cos\theta_m\hat{\mathbf{x}}+\cos\phi_m\cos\theta_m\hat{\mathbf{y}}+\sin\theta_m\hat{\mathbf{z}}$. Taking the scalar product of this vector with the force in Eq. (6) gives the polar component of the dipolar force,

$$F_\theta = -2f_c\cos\alpha(\cos\theta_f\sin\theta_m - \sin\theta_f\cos\theta_m\cos\phi_m). \tag{8}$$

When inertial effects are negligible (we discuss this condition below), stationary orbits occur when this polar force is zero, a condition that obtains when

$$\tan\theta_m = \cos\phi_m\tan\theta_f. \tag{9}$$

This closure relation can be used to simplify Eq. (7), as well as subsequent relations in this paper. For stationary orbits the chain-field angle can be expressed as

$$\cos\alpha = \frac{\cos\theta_f}{\cos\theta_m}. \tag{10}$$

Useful equivalent forms of this closure relation include $\sin\alpha=\sin\theta_f\sin\phi_m$ and $\sin 2\alpha=\sin 2\theta_f\sin\phi_m/\cos\theta_m$.

A plot of the locus of stationary orbits (values of ϕ_m and θ_m) for selected vortex field angles is given in Fig. 2. For all vortex field angles it is apparent that, as the chain phase lag increases, the polar chain angle decreases, eventually reaching zero when the phase lag reaches 90°. Thus as the field frequency increases, the chains tend to align along the z axis, where they become immobile—a catastrophe for mixing. In the following we shall see that this mixing catastrophe is prevented by factors that limit the stability of chains in stationary orbits.

Azimuthal and radial dipolar forces

An expression for the azimuthal force $F_\phi=\mathbf{F}\cdot\hat{\boldsymbol{\phi}}$ is needed to determine the phase lag of the chain as a function of

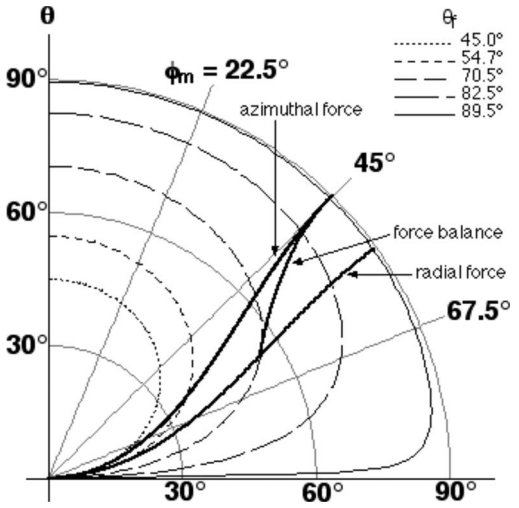

FIG. 2. A polar plot of the locus of stationary orbits of chains following a vortex field. The radial distance is the polar angle θ and the chain phase lag ϕ_m is the azimuthal angle. At constant field magnitude, ramping up the field frequency will cause the chain phase lag to increase and the chain polar chain angle to decrease, until the stationary orbit hits one of the three stability limits, at which point the chain can or will fragment. Without these instabilities vortex mixing would not occur, because the chains could aggregate without limit and align with the mixing axis.

experimental conditions. This force is obtained by noting that $\hat{\boldsymbol{\phi}}=\cos\phi_m\hat{\mathbf{x}}-\sin\phi_m\hat{\mathbf{y}}$, with the result

$$F_\phi = -2f_c\cos\alpha\sin\theta_f\sin\phi_m. \tag{11}$$

For stationary orbits Eq. (9) can be used to simplify this force to

$$F_\phi = -f_c\sin 2\alpha, \tag{12}$$

where we recall that for stationary orbits $\sin 2\alpha=\sin 2\theta_f\sin\phi_m/\cos\theta_m$. For stationary orbits the implicit dependence of Eq. (12) on the polar angle θ_m can be eliminated using

$$\cos\theta_m = \frac{\cos\theta_f}{\sqrt{\cos^2\theta_f + \sin^2\theta_f\cos^2\phi_m}}, \tag{13}$$

which is a variant of Eq. (9). The azimuthal dipolar force can then be expressed as

$$F_\phi = -f_c\times 2\sin\theta_f\sin\phi_m\sqrt{\cos^2\theta_f + \sin^2\theta_f\cos^2\phi_m}. \tag{14}$$

A plot of the azimuthal force as a function of the phase lag is given in Fig. 3(a) for a range of vortex field angles. Most interesting is that for vortex field angles greater than 45° this force has a maximum at a phase lag smaller than 90°. We will discuss the significance of this maximum in the section on the stability of orbits below.

The radial component of the dipolar force, $F_r=\mathbf{F}\cdot\hat{\mathbf{r}}$, is important to the stability of a chain. The radial force is obtained using $\hat{\mathbf{r}}=\sin\phi_m\sin\theta_m\hat{\mathbf{x}}+\cos\phi_m\sin\theta_m\hat{\mathbf{y}}+\cos\theta_m\hat{\mathbf{z}}$ and for stationary orbits is

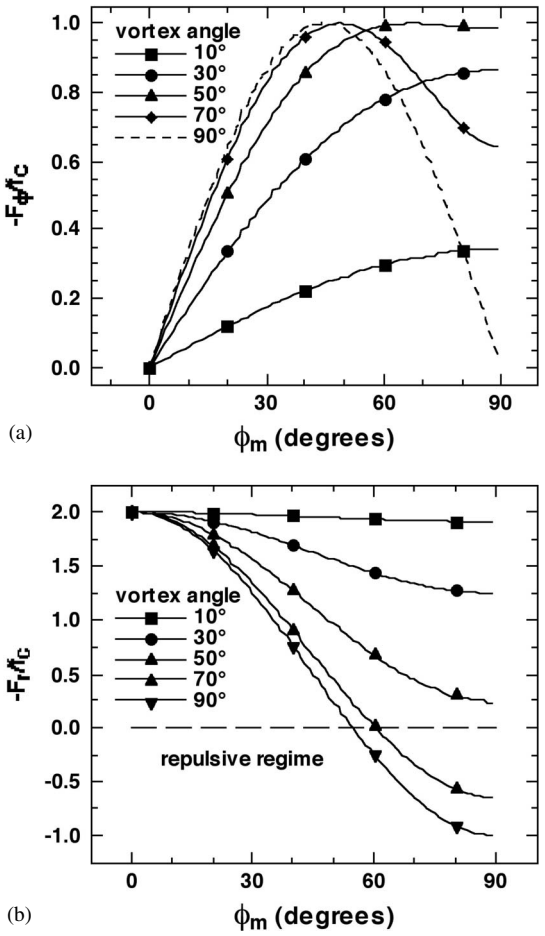

FIG. 3. (a) The dependence of the azimuthal force on phase lag is given for a range of values of the vortex field angle. Note that for vortex field angles greater than 45° the force is nonmonotonic. (b) The radial component of the force becomes repulsive for large phase lags when the vortex field angle exceeds ~54.7°.

$$F_r = -f_c(3\cos^2\alpha - 1). \tag{15}$$

Using Eqs. (10) and (13), this force can be expressed as

$$F_r = -f_c[3(\cos^2\theta_f + \sin^2\theta_f \cos^2\phi_m) - 1]. \tag{16}$$

A plot of this force as a function of phase lag is given in Fig. 3(b). For vortex field angles smaller than ~54.7° this force is always attractive for stable stationary orbits; for larger vortex field angles the force will become repulsive at a critical phase lag, and so orbits with phase lags larger than this cannot exist.

In summary, for stationary orbits the dipolar force can be expressed as $\mathbf{F} = -f_c[(3\cos^2\alpha - 1)\hat{\mathbf{r}} + \sin 2\alpha\hat{\boldsymbol{\phi}}]$. This equation is of the same form as Eq. (5), because for stationary orbits the dipole moments lie in the plane of the chain and the field.

Hydrodynamic force

The hydrodynamic tension between the central pair of particles in a chain is a sum over the individual hydrodynamic forces on the particles on either side of the chain. (The situation is analogous to a tug of war, where the tension in the middle of the rope is computed from the tugs on either end of the rope.) The hydrodynamic force on a particle of radius a is $-6\pi\eta a\mathbf{v}$, where $\mathbf{v}$ is the relative velocity of the particle against the liquid. Because the angular velocity of the fluid is negligible compared to the frequency of the rotating field, $\mathbf{v}$ is to a good approximation the particle velocity. For a vortex field whose x-y component is rotating in the direction of $-\hat{\boldsymbol{\phi}}$, the velocity of particle j is $\mathbf{v}_j = -\omega R_j\hat{\boldsymbol{\phi}}$, where $R_j = (2j-1)a\sin\theta_m$ is the distance of the particle from the z axis. The hydrodynamic force on particle j is thus

$$\mathbf{F}_{h,j} = 6\pi\eta a^2\omega(2j-1)\sin\theta_m\hat{\boldsymbol{\phi}}. \tag{17}$$

The azimuthal force between the central particles in the chain is due to the total hydrodynamic drag on each half chain,

$$\mathbf{F}_h = \sum_{j=1}^{N}\mathbf{F}_{h,j} \cong 6\pi\eta\omega a^2N^2\sin\theta_m\hat{\boldsymbol{\phi}}. \tag{18}$$

This hydrodynamic force increases as the square of the length $4aN$ of the chain and is independent of its width. Use of Eq. (13) to eliminate the polar angle gives

$$\mathbf{F}_h = 6\pi\eta\omega a^2N^2\frac{\sin\theta_f\cos\phi_m}{\sqrt{\cos^2\theta_f + \sin^2\theta_f\cos^2\phi_m}}\hat{\boldsymbol{\phi}}, \tag{19}$$

which is valid only for chains in stationary orbits. A plot of the hydrodynamic drag as a function of the phase lag is given in Fig. 4(a) for various values of the vortex field angle. As the vortex field angle approaches 90° this force becomes independent of the phase lag, as it must.

Inertia

Before we compute the chain phase lag, which requires a balance between magnetic and hydrodynamic forces, it is worth estimating the magnitude of centrifugal forces, since if these are significant they could increase the polar angle of the chain orbits. The centrifugal force on a particle is $F_{\text{cent}} = \omega^2 R_j v_p\Delta\rho$, where $\Delta\rho$ is the difference between the density of the particles and the fluid and v_p is the volume of a particle. Comparison of this force to the hydrodynamic force on a particle gives $F_{\text{cent}}/F_h = \omega a^2\Delta\rho/9\eta$. Take as a typical example 10 μm Fe particles in water (viscosity of 1 kPa) at a field frequency of 1 kHz. In this case this force ratio is 4×10^{-9}, so centrifugal forces need not be considered. We will ignore centrifugal forces in this paper, with the understanding that they could become important for very large particles and field frequencies, and low fluid viscosities.

Phase lag

The chain phase lag ϕ_m is determined by a balance between the azimuthal dipolar and hydrodynamic forces. Use of Eqs. (14) and (19) gives

$$(\cos^2\theta_f + \sin^2\theta_f\cos^2\phi_m)\tan\phi_m = 8\,\text{Mn}\,N^2. \tag{20}$$

To derive this expression we have used $f_c = (\pi/12)a^2\mu_0M^2$ for the force amplitude between contacting particles, where

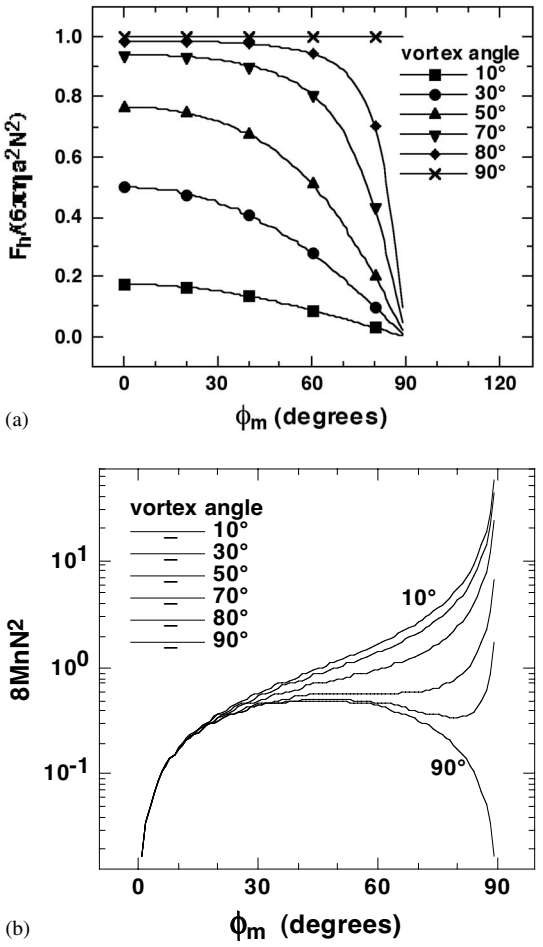

FIG. 4. (a) The hydrodynamic force decreases with phase lag, because of the concomitant decrease in the polar angle. (b) The product of the Mason number and the square of the chain size as a function of phase lag. At higher vortex field angles several phase lags are possible, but only one corresponds to a stable orbit.

M is the magnetization of a particle, and have defined the Mason number as $\mathrm{Mn}=9\eta\omega/(2\mu_0 M^2)$. At low fields the magnetization is linear in the field, $\mathbf{M}=\chi_p\mathbf{H}_0$, where $\chi_p=3\beta$ is the particle susceptibility in terms of the contrast factor $\beta=(\mu_p-\mu_c)/(\mu_p+2\mu_c)$, which is a function of the permeabilities μ_p,μ_c of the particle and continuous phases. In this low-field limit $\mathrm{Mn}=\eta\omega/(2\mu_0\beta^2H_0^2)$. It should be noted that Eq. (20) gives the correct result, $\sin 2\phi_m=16\mathrm{Mn}N^2$, for the limiting case of a rotating field ($\theta_f=90°$) [5].

Equation (20) is plotted in Fig. 4(b) for a range of vortex field angles. On the basis of this plot alone it would appear that for vortex field angles greater than ~70° there are three possible stationary orbits for a chain. Also, for smaller vortex field angles it would appear that chains of infinite length can form. We shall show that these divergent chains form along the z axis, and make a negligible contribution to mixing.

Stability

Azimuthal force

At this point we need to determine whether a chain in a particular stationary orbit is stable. The first issue is the azimuthal dipolar force, Eq. (14), which Fig. 3(a) indicates can have a maximum at some phase lag ϕ_m^* for vortex field angles exceeding 45°. In the large-phase-lag regime where the derivative of $-F_\phi$ is negative, a fluctuation of a chain to a larger phase lag will reduce the magnetic torque, which could lead to a further increase in the phase lag, and a further reduction in the magnetic torque, possibly leading the chain out of a stationary orbit, and into a regime where the radial component of the dipolar force becomes repulsive, i.e., the angle of the chain relative to the field exceeds ~54.7°.

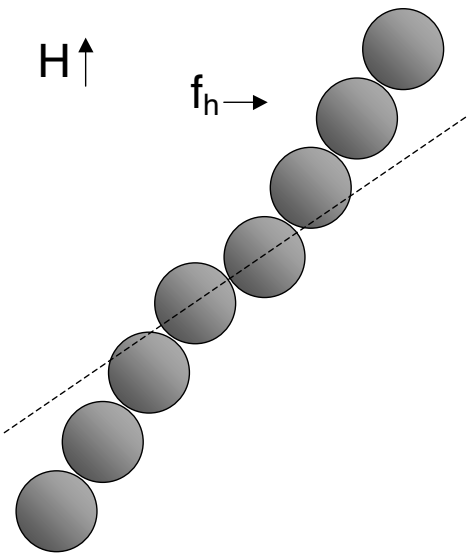

FIG. 5. An example of a fluctuation that can lead to chain fragmentation due to the local maximum in the azimuthal force. In this case the angle between particles at the chain center has fluctuated to a value where the derivative of the azimuthal force with respect to the azimuthal angle is negative. The hydrodynamic force on each semichain has not decreased, however, so the hydrodynamic force dominates the azimuthal force, and the angle between particles at the chain center will increase until the radial dipolar force becomes repulsive and the chain fragments.

The phase lag ϕ_m^* where the azimuthal force maximizes can be computed by setting $dF_\phi/d\phi=0$, with the result

$$\sin\phi_m^*=\frac{1}{\sqrt{2}\sin\theta_f}\quad\text{for }\theta_f\geqslant 45°, \tag{21}$$

which is plotted in Fig. 2. For vortex field angles smaller than 45° the maximum phase lag is 90°, so in this case all orbits are stable. Chains with phase lags below ϕ_m^* are in stable stationary orbits, because a fluctuation that increases the phase lag also increases the magnetic torque, which then drives the chain back to a smaller phase lag. For a balanced vortex field $\sin\phi_m^*=\sqrt{3/4}$, so in this case orbits with phase lags up to 60° are stable to fluctuations in phase lag.

This azimuthal force stability condition would lead to chain fracture for certain thermal fluctuations. For example, suppose a fluctuation occurred where at the chain center the azimuthal angle between particles increased beyond ϕ_m^* whereas the azimuthal angle of the two chain halves did not change (see Fig. 5). This fluctuation would lead to chain

fracture because the hydrodynamic force on the chain halves is constant, whereas the azimuthal force is decreasing with increasing phase lag. Equation (21) is thus a condition of chain metastability.

It is interesting to compute the polar angle θ_m^* of the critical chains in orbits with phase lag ϕ_m^*. Combining Eqs. (9) and (21) gives

$$\sin \theta_m^* = \sqrt{\sin^2 \theta_f - \cos^2 \theta_f} \quad \text{for } \theta_f \geqslant 45\,^\circ. \tag{22}$$

For vortex field angles of 45° or less, the critical polar angle is 0°, so critical chains are aligned with the z axis, and therefore do not create mixing torque. This polar angle then increases progressively with vortex field angle, as is evident from Fig. 2, and prevents a mixing catastrophe from occurring for vortex field angles exceeding 45°.

Radial force

A second condition for chain stability is that the radial component of the dipolar force, Fig. 3(b), between enchained particles is attractive. From Eq. (16) it can be shown that for a chain in a stationary orbit the radial force becomes repulsive for phase lags greater than ϕ_m^{**}, where

$$\sin \phi_m^{**} = \frac{1}{\sqrt{3/2} \sin \theta_f} \quad \text{for } \theta_f \geqslant 54.7\,^\circ. \tag{23}$$

Chains will rupture when this phase lag is exceeded, so Eq. (23) is a true stability limit, because it leads to rupture in the absence of fluctuations. This mechanism of chain rupture is not a consideration for stationary orbits in fields with vortex angles smaller than 54.7°. Comparison of this critical angle for the radial force to the critical angle for the azimuthal force, Fig. 2, shows that $\phi_m^* \leqslant \phi_m^{**}$. Chains with intermediate phase lags are at most metastable.

Force balance

Finally, for vortex field angles greater than ~70.5° there can be multiple solutions (phase lags) to the force balance condition, Eq. (20), as shown in Fig. 4(b). Phase lags where the slope of this function is negative correspond to unstable orbits. Differentiation of Eq. (20) with respect to the phase lag gives

$$\cos \phi_m \sqrt{\sin^2 \phi_m - \cos^2 \phi_m} = \cot \theta_f, \tag{24}$$

and solutions to this give the positions of the local maxima, $\phi_{\max}$, and minima, $\phi_{\min}$, in Fig. 4(b). The positions of the maxima, $\phi_{\max}$, lie between ϕ^* and ϕ^{**} (see Fig. 2), so if a chain somehow found itself in a stationary orbit with a phase lag greater than $\phi_{\max}$ the phase lag would increase until the chain ruptured.

Stability regimes

We have identified three causes of chain instability. How and whether these instabilities lead to fracture depends on the vortex field angle, as shown in Fig. 2. There are four distinct instability regimes.

(1) $\theta_f \leqslant 45°$: In this regime there are no instabilities along the locus of stationary orbits. As the phase lag of a chain increases to 90° the polar angle will collapse to zero. These z-aligned chains can grow without limit and will not contribute to the mixing torque. In this regime mixing is not expected.

(2) $45° < \theta_f \leqslant 54.7°$: For vortex angles in this regime the locus of stationary orbits intersects the azimuthal force instability, Eq. (21). Chains with phase lags larger than ϕ_m^* are metastable, and subject to fragmentation due to fluctuations. These fluctuations might be thermal, or due to fluctuations in the flow field at the chain. This process will prevent chains from aligning with the z axis, so mixing is expected.

(3) $54.7° \leqslant \theta_f \leqslant 70.5°$: In this regime the locus of stationary orbits intersects the radial force instability given in Eq. (23). When the critical phase lag ϕ_m^{**} is reached the chain will become unstable and will immediately rupture. Because chains cannot align with the z axis, mixing is expected.

(4) $70.5° < \theta_f \leqslant 90°$: Here the locus of stationary orbits intersects the force balance instability, Eq. (24), before intersecting the radial force instability. When the phase lag of a chain increases to a value slightly greater than $\phi_{\max}$ the hydrodynamic force will dominate the dipolar force, causing the phase lag to continuously increase until the radial instability is encountered, at which point the chain will immediately rupture. Mixing for a suspension of chains is again expected, but only if the solution consists of chains. There is a strong tendency for particles to form sheets, not chains, at high vortex angles; however, chains can be made by initially applying a static field.

Simulations

To verify the analytical results we have derived thus far we conducted a dynamical simulation of a chain in a vortex field. This simulation is done at the same level of approximation as the theory: the dipole moments of the spherical particles are fixed and they experience Stokes drag as they move relative to the surrounding fluid. Thermal fluctuations are not included. The locus of stable stationary orbits is swept out by slowly ramping up the vortex field frequency at fixed field amplitude. The results, shown in Fig. 6, are in agreement with the analytic expressions we have obtained. The orbits are those predicted by Eq. (9) until the radial or force balance stability conditions cause the chain to fragment. The azimuthal force instability does not come into play because the simulation does not incorporate thermal fluctuations.

Maximum chain size

An expression for the maximum size of a chain in a stable orbit is required to compute the mixing torque. This maximum size can be obtained by substituting Eq. (21) into Eq. (20), with the result

$$N_{\max}^2 = \frac{1}{16\mathrm{Mn}\sqrt{\sin^2 \theta_f - \cos^2 \theta_f}} \quad \text{for } \theta_f \geqslant 45\,^\circ. \tag{25}$$

Note that the maximum stable chain size diverges to infinity as the vortex field angle approaches 45° from above, as shown in Fig. 7, and for angles near 45° the divergence

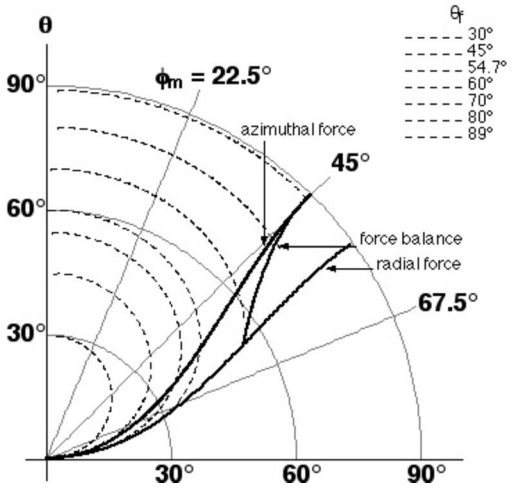

FIG. 6. Dynamical simulations of a chain in a vortex field show that the locus of stable orbits agrees with the analytical results plotted in Fig. 2. The force balance and radial instabilities cause chain fragmentation, thus preventing the chains from aligning with the mixing axis. It is because of these instabilities that mixing occurs in vortex magnetic fields.

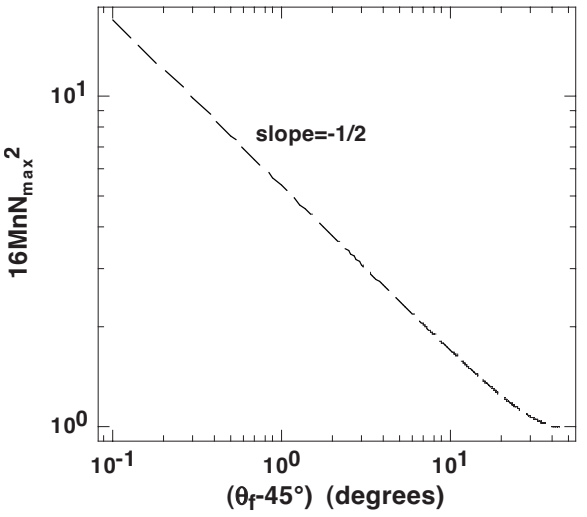

FIG. 7. The maximum chain length diverges as $N_{\max}^2 \sim (\theta_f - \pi/4)^{-1/2}$ as the vortex field angle approaches 45° from above. This shows that vortex field angles smaller than 45° simply produce chains and are not expected to be effective at mixing.

scales like $N_{\max}^2 \sim (\theta_f - \pi/4)^{-1/2}$. Equation (22) shows that these infinite chains would be aligned along the z axis.

This expression for the maximum chain length allows the computation of the critical Mason number Mn* for stable chain formation in a vortex field. For Mason numbers larger than this, chains cannot form and magnetic mixing will not occur. This stagnation can occur because the field is too low, the field frequency is too high, or the liquid viscosity is too large. This critical Mason number will occur when particle pairs can just exist at the largest tangential force for a stable orbit. Substituting $N_{\max}=1$ (which corresponds to a particle pair) into Eq. (25) gives

$$\mathrm{Mn}^* = \frac{1}{16\sqrt{\sin^2\theta_f - \cos^2\theta_f}} \quad \text{for } \theta_f \geqslant 45\,^\circ. \tag{26}$$

For vortex field angles of 45° or less, the critical Mason number is of course infinite, because stationary chains can form along the z axis. For a balanced vortex field the critical Mason number is $\mathrm{Mn}^* = \sqrt{3}/16 \cong 0.108$.

Mixing torque

The mixing torque can be computed by summing the product of the hydrodynamic force on each particle times its distance R from the z axis, which is the mixing axis. From Eq. (17) the hydrodynamic torque on a single chain can be written

$$\tau_h = \sum_{j=-N}^{N} f_{h,j} R_j \cong 2\pi\eta\omega L^3 \sin^2\theta_m, \tag{27}$$

where $2L$ is the length of the chain. (Note that the hydrodynamic torque does not depend on the width of the chain.) The mixing torque density T is the hydrodynamic torque per unit volume. The number of chains per unit volume is $n_{\mathrm{ch}} = \phi/(2NV_p)$ where ϕ_p is the volume fraction of particles and V_p is the volume of a particle. The mixing torque density is thus

$$T = n_{\mathrm{ch}}\tau = 6\eta\omega\phi_p N^2 \sin^2\theta_m. \tag{28}$$

The chain size N can be eliminated from this expression by using $8\,\mathrm{Mn}\,N^2 = \sin 2\theta_f \sin\phi_m / \sin 2\theta_m$ to obtain $T = \frac{1}{12}\phi\mu_0 M^2 \sin 2\theta_f \sin\phi_m \tan\theta_m$. Using the stationary orbit condition Eq. (9), we can eliminate θ_m to obtain

$$T = \frac{1}{12}\phi_p\mu_0 M^2 \sin^2\theta_f \sin 2\phi_m. \tag{29}$$

Chains will tend to aggregate to their maximum stable length, in which case the metastability condition in Eq. (21) can be used to eliminate the phase lag, giving

$$T = \frac{1}{12}\phi_p\mu_0 M^2 \sqrt{\sin^2\theta_f - \cos^2\theta_f} \quad \text{for } \theta_f \geqslant 45\,^\circ. \tag{30}$$

The mixing torque density is thus expected to be zero until the vortex angle reaches 45°. In the region where the torque density is expected to be zero, the critical Mason number is infinity, and in this regime chains will tend to aggregate and align with the z axis.

Equation (30) has some interesting aspects. First, the torque density is expected to be independent of the particle size, which makes this method of mixing scalable to microfluidics devices. Second, in the regime below the critical Mason number the torque density is expected to be independent of the fluid viscosity. Third, in this regime the torque density is predicted to be independent of the field frequency. [Of course, if the field frequency is quite low, the calculated maximum chain size in Eq. (26) will exceed the size of the mixing volume, and this will reduce the torque density.] This independence of the torque on field frequency is a manifestation of the well-known shear thinning rheology of magnetorheological and electrorheological fluids. Fourth, this equa-

tion predicts substantial torque at large vortex field angles, even maximizing at a rotating field. But at reasonable particle concentrations and field frequencies this is not observed, because the particles form sheets, not chains. Finally, the torque predicted by Eq. (30) for a balanced triaxial field is only 25% of the torque we measure [3]. To some extent this discrepancy is due to the fact that the fields we apply are low enough to make the dipolar contribution to the local field significant compared to the applied field.

Self-consistent point dipoles

Up to this point we have worked in the simplifying, high-field approximation that the local field at each dipole is dominated by the applied field. This is a poor approximation at low applied fields, where the contributions to the local magnetic field from the other dipoles in the suspension are important. By far the largest contribution to the local field at a particular dipole comes from the other dipoles in the same chain, so we will focus exclusively on these contributions.

The attractive dipole interaction between two contacting particles in the interior of a long chain can be computed from a self-consistent local field treatment of point dipoles [4], with the result

$$\mathbf{F}_d = -f_c\zeta(3)[(3\kappa_1\cos^2\alpha - \kappa_2)\hat{\mathbf{r}} + \kappa_3 \sin 2\alpha\hat{\boldsymbol{\alpha}}]. \quad (31)$$

Here $\kappa_1=(1+\frac{1}{8}\xi^2)/(1-\frac{1}{4}\xi-\frac{1}{8}\xi^2)^2$, $\kappa_2=1/(1+\frac{1}{4}\xi)^2$, $\kappa_3=1/(1-\frac{1}{4}\xi-\frac{1}{8}\xi^2)$, and the variable $\xi=\beta\zeta(3)$, in terms of the Rieman zeta function $\zeta(3)\sim 1.202$.

Equation (31) is written in terms of the angle α of a chain in a stationary orbit to the applied field. This can be done because the dipoles lie in the plane defined by the chain axis and the field. The azimuthal component of the force, $F_\phi(\beta)$, is larger by a factor of $\zeta(3)\kappa_3$ than the bare interaction force F_ϕ of Eq. (12), or simply $F_\phi(\beta)=\kappa_3\zeta(3)F_\phi$. This simple renormalization of the azimuthal force does not affect the stability condition in Eq. (21), nor the force balance condition in Eq. (24). The radial component of the force changes significantly, and it is easy to show that the interactions between particles in a chain become repulsive when

$$\sin\phi^{**} = \frac{\sqrt{1-\kappa_2/3\kappa_1}}{\sin\theta_f}. \quad (32)$$

For particles with positive permeability contrast with the liquid (i.e., magnetic particles in a nonmagnetic liquid) the effect of the local field is to increase the angle where the interparticle interactions become repulsive. Thus Eq. (21) remains the dominant instability. For the case of strong negative contrast ($\beta=-0.5$) Eq. (32) becomes the dominant instability, but the effect of dipolar fields is slight. (Negative contrast could be achieved by adding dielectric spheres, such as silica, to a ferrofluid.)

For the case of positive contrast the maximum chain length, Eq. (25), becomes

$$16\,\mathrm{Mn}\,N_{\max}^2 = \kappa_3\zeta(3)/\sqrt{\sin^2\theta_f - \cos^2\theta_f} \quad \text{for } \theta_f \geqslant 45°, \quad (33)$$

so accounting for the local field increases the predicted chain length. Substituting this new maximum chain length expression into Eq. (28) gives for the torque density

$$T = \frac{1}{12}\kappa_3\zeta(3)\phi_p\mu_0 M^2\sqrt{\sin^2\theta_f - \cos^2\theta_f} \quad \text{for } \theta_f \geqslant 45°. \quad (34)$$

For $\beta=1$ the factor $\kappa_3\zeta(3)\cong 2.32$, so the torque density is considerably larger when local fields effects are accounted for in positive-contrast systems. The torque density diminishes for the more exotic negative-contrast case, and although it is straightforward to show this, the algebra is very messy, since Eq. (32) becomes the dominant instability.

The critical Mason number is also affected by the local field. We recall that the critical Mason number is defined as that value above which a chain of two dipoles cannot exist. Equation (31) applies *only* to long chains, and so we must now compute the angular force between just two particles self-consistently. The result (see the Appendix) is

$$\mathbf{F}_\alpha = -f_c\lambda_3 \sin 2\alpha\,\hat{\boldsymbol{\alpha}}, \quad (35)$$

where $\lambda_3=1/(1-\beta/8-\beta^2/32)$. The critical Mason number can then be shown to be

$$\mathrm{Mn}^* = \frac{\lambda_3}{16\sqrt{\sin^2\theta_f - \cos^2\theta_f}} \quad \text{for } \theta_f \geqslant 45°, \quad (36)$$

which is numerically similar to Eq. (26), since even for $\beta=1$ the value of λ_3 is only 1.19. In summary, the effect of local fields is to increase the mixing torque significantly and to increase the critical Mason number slightly.

MAGNETIC MIXING WITH RODS

In this section we compare the results we have obtained for particle chains to the corresponding results for magnetically soft rods. There are some obvious differences. In the case of particle chains, the magnetic forces are due to dipolar interactions between particles, and the chains are volatile, adaptive agglomerates. For rods, the magnetic torque is due to the cross product of the magnetic moment with the applied field, and the rod size is fixed. (Rods might also agglomerate, but here we consider only single rods.) In the following we will consider rods only in the low-field regime where the magnetic moment is proportional to the field.

Magnetic moment

If a rod has a very large aspect ratio, and is made of a high-permeability material, such as pure iron, then a consideration of the relevant demagnetization factors shows that the rod will magnetize strongly only along its length. In fact, in the large-aspect-ratio limit the apparent susceptibility of a rod along its length will be the material susceptibility (easily 10^3–10^4) whereas perpendicular to its length the apparent susceptibility will not exceed 2. Therefore, to a good approximation we can write the moment of a rod as

$$\mathbf{m} = pH_0(\hat{\mathbf{h}}\cdot\hat{\mathbf{r}})\hat{\mathbf{r}}, \quad (37)$$

where $\hat{\mathbf{r}}=\sin\phi_m\sin\theta_m\hat{\mathbf{x}}+\cos\phi_m\sin\theta_m\hat{\mathbf{y}}+\cos\theta_m\hat{\mathbf{z}}$ is a unit vector along the rod, $\hat{\mathbf{h}}=\sin\theta_f\hat{\mathbf{y}}+\cos\theta_f\hat{\mathbf{z}}$ is a unit vector

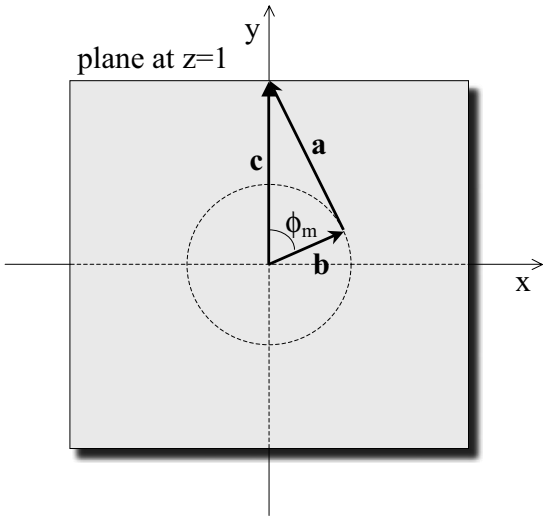

FIG. 8. Diagram showing the vectors **a**, **b**, and **c** for calculating the stable orbits of rods. The vector **a** lies in the *x*-*y* plane, and the vectors **b** and **c** are of unit height.

along the applied field, and p is the polarizability of the rod along its length. The product $\hat{\mathbf{h}}\cdot\hat{\mathbf{r}}=\cos\alpha=\cos\phi_m\sin\theta_m\sin\theta_f+\cos\theta_m\cos\theta_f$, where α is the angle between the rod and the field.

Stationary orbits

A stationary orbit will occur when the hydrodynamic and magnetic torques are aligned. The magnetic torque is due to the interaction of the rod magnetic moment with the field, $\boldsymbol{\tau}_m=\mu_0\mathbf{m}\times\mathbf{H}_0$. This torque is perpendicular to the plane of the vectors $\hat{\mathbf{h}}$ and $\hat{\mathbf{r}}$, whereas the hydrodynamic torque is perpendicular to the vectors $\hat{\boldsymbol{\phi}}$ and $\hat{\mathbf{r}}$. For the hydrodynamic torque to be aligned with the magnetic torque thus requires the vector $\hat{\boldsymbol{\phi}}$ to be in the $\hat{\mathbf{h}}$-$\hat{\mathbf{r}}$ plane.

With this requirement in mind, the condition for a stationary orbit can be derived with reference to Fig. 8. Define the vectors of unit height $\mathbf{b}=\hat{\mathbf{r}}/\cos\theta_m$ and $\mathbf{c}=\hat{\mathbf{h}}/\cos\theta_f$. Then let $\mathbf{a}=\mathbf{c}-\mathbf{b}$. This vector $\mathbf{a}$ is the intersection of the $\hat{\mathbf{h}}$-$\hat{\mathbf{r}}$ plane with a plane parallel to the *x*-*y* plane. For the vector $\mathbf{a}$ to be parallel to $\hat{\boldsymbol{\phi}}$ requires $\mathbf{b}\cdot\mathbf{a}=0$, which gives the stationary orbit condition

$$\tan\theta_m=\cos\phi_m\tan\theta_f. \tag{38}$$

This is the same condition as derived for the chain, and so once again we obtain the relation $\cos\alpha=\cos\theta_f/\cos\theta_m$ for the angle between the rod and the field.

Torque balance

The magnitude of the magnetic torque is $\tau_m=\mu_0|\mathbf{m}\times\mathbf{H}_0|=\mu_0 mH_0\sin\alpha$. For low fields the magnitude of the dipole moment is $m=pH_0\cos\alpha$ where the polarizability $p=V_r\chi_\parallel$ in terms of the rod volume V_r and the susceptibility parallel to the rod, $\chi_\parallel$. The magnetic torque can thus be expressed as

$$\tau_m=\frac{1}{2}\mu_0 V_r\chi_\parallel H_0^2\sin 2\alpha, \tag{39}$$

which has the same angular dependence as the chain force in Eq. (12). From this it is clear that the maximum rod torque will be reached at the critical phase lag given by Eq. (21), which thus marks a limit of stability for rod orbits.

A proper consideration of the hydrodynamic torque of a rod gives an expression with a logarithmic dependence on the rod aspect ratio. A simple and accurate approximation is to consider the rod as a rigid, immutable chain of spheres. The hydrodynamic torque on the rod is then given by summing the force on each sphere, Eq. (17), times its moment around the instantaneous axis of rod rotation, which for stationary orbits we recall is parallel to the rotation axis of the magnetic torque. This moment is simply the distance to the jth sphere, $(2j-1)a$. The hydrodynamic torque around this axis is thus

$$\tau_h=\sum_{-N}^{N}6\pi\eta a^3\omega(2j-1)^2\times\sin\theta_m=2\pi\eta L^3\omega\sin\theta_m, \tag{40}$$

where L is the half length of the rod. Balancing the torques in Eqs. (39) and (40) gives

$$(\cos^2\theta_f+\sin^2\theta_f\cos^2\phi_m)\tan\phi_m=\frac{\eta\omega}{\mu_0\chi_\parallel H_0^2}N_r^2 \tag{41}$$

for the phase lag of the rod, where N_r is the aspect ratio of the rod. (Note the similarity of this result to Eq. (20) for the chain.) The prefactor $\eta\omega/(\mu_0\chi_\parallel H_0^2)$ is a Mason number for the rod problem.

A rod will reach a stagnation point if the field frequency becomes too large or the field amplitude becomes too small. This point will obtain when the torque decreases with increasing phase lag, as given by Eq. (21). Substitution of Eq. (21) into Eq. (41) shows that this stagnation condition is given by

$$\frac{2\eta\omega}{\mu_0\chi_\parallel H_0^2}N_r^2\geqslant\frac{1}{\sqrt{\sin^2\theta_f-\cos^2\theta_f}}\quad\text{for }\theta_f\geqslant 45°. \tag{42}$$

For vortex field angles smaller than 45° the stagnation phenomenon will not occur, since a rod can simply align along the vertical axis as the field frequency is increased. For a balanced triaxial field the stagnation point is $2\eta\omega N_r^2/(\mu_0\chi_\parallel H_0^2)\geqslant 1/\sqrt{3}$.

Mixing torque

The mixing torque of a rod is the torque around the vertical axis, $2\pi\eta L^3\omega\sin^2\theta_m$, which is smaller by a factor of $\sin\theta_m$ than the torque in Eq. (40). For a suspension containing a volume fraction ϕ_r of rods, the torque density is

$$T=\eta\omega\phi_r N_r^2\frac{\sin^2\theta_f\cos^2\phi_m}{\cos^2\theta_f+\sin^2\theta_f\cos^2\phi_m}. \tag{43}$$

Equation (41) can be used to express this torque in magnetic units, with the result

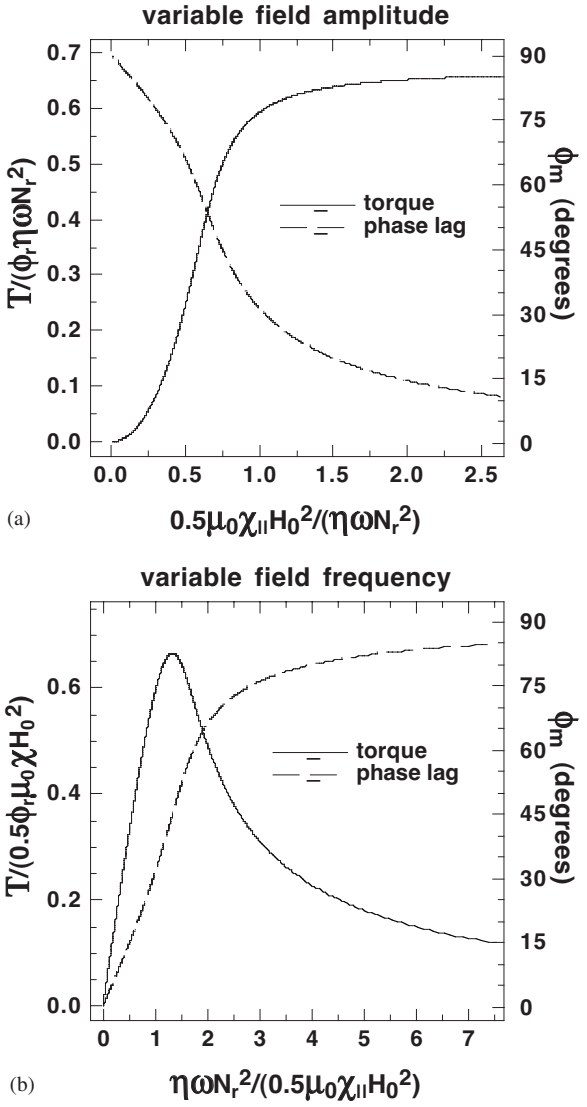

FIG. 9. Plots of the mixing torque of a solution of rods in a balanced vortex field ($\theta_f \sim 54.7°$), where orbits with phase lags greater than 60° are unstable. (a) Here the field frequency is fixed and the field amplitude is varied. The torque increases continuously with field amplitude, then saturates at low phase lag as the polar chain angle θ_m reaches its maximum value θ_f. This continuous torque increase cannot occur in a simple rotating field. (b) If the field amplitude is fixed and the frequency is varied, the mixing torque increases nearly linearly with the torque at low frequencies, and then falls off continuously.

$$T = \frac{1}{2}\mu_0 \phi_r \chi_\parallel H_0^2 \sin^2 \theta_f \sin 2\phi_m, \tag{44}$$

which can be compared to Eq. (29) for chains.

It is interesting to examine the mixing torque density as a function of field frequency and amplitude. For a rod in a rotating field (vortex angle of 90°) the behavior is quite simple: the torque is proportional to the field frequency and independent of the amplitude until stagnation occurs, at which point the mixing torque abruptly drops to zero. Stagnation occurs at high frequency and/or low fields. Equations (43) and (44) seem not to hint at this behavior, but a consideration of the phase lags involved demonstrate this instability, as we now discuss.

Plots of the mixing torque density can be made by solving Eq. (41) to determine the phase lag of a stationary orbit for any particular experimental conditions, then substituting this into Eq. (43) or (44) to compute the mixing torque density. For an experiment at fixed field frequency and variable field amplitude, this process yields the results in Fig. 9(a) for a vortex field angle of 54.7°. As the field increases, the phase lag decreases to zero and the mixing torque reaches a maxi-

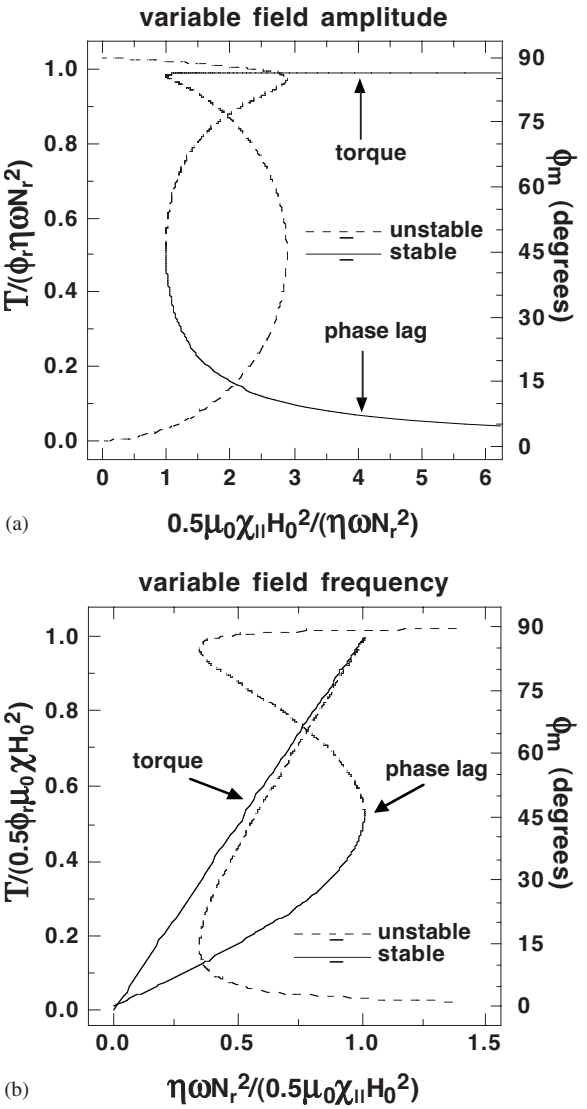

FIG. 10. Plots of the mixing torque of a solution of rods in a vortex field of angle θ_f=85°, where orbits with phase lags greater than ~45.2° are unstable. (a) In a variable field amplitude plot the mixing torque is very nearly constant at high fields. As the field is lowered, an instability develops at a phase lag of 45.2°, whereupon the torque drops to zero. (b) In a variable field frequency plot the mixing torque increases linearly with the field until a phase lag of 45° is reached. At ~45.2° phase lag the instability will drive the torque abruptly to zero. In each plot the solid lines denote the stable regime, $\phi_m < 45.2°$, and the dashed lines denote the unstable regime, $\phi_m > 45.2°$.

mum. The increase is not linear, but is sigmoidal in shape. (Note that these plots are made without regard to the stability conditions that make orbits with large phase lags unstable.) In Fig. 9(b) the corresponding results are given for an experiment at constant field, but variable field amplitude. The mixing torque reaches a maximum at the frequency where the phase lag is 45°, as expected from Eq. (44), and then falls off gradually.

The results become much more interesting at large vortex field angles. At a vortex angle of 90° the torque must increase in proportion to the field frequency, and be independent of the field amplitude, until stagnation occurs. Figure 10 shows how a continuous transition to this simple behavior occurs with increasing vortex angle. As expected, Fig. 10(a) shows that in an experiment where the field is varied the torque is very nearly independent of field until the field becomes small enough that the phase lag increases to the point where an instability occurs. Likewise, Fig. 10(b) shows that for an experiment at variable frequency the increase is linear until the instability is reached, whereupon stagnation will occur.

CONCLUSIONS

We have developed expressions for the mixing torque density of suspensions of magnetic rods and particles subjected to vortex magnetic fields. The results for chains are in good agreement with laboratory observations: the torque is quadratic in the applied field, and independent of the field frequency and fluid viscosity over a wide range. This theory also predicts that the mixing torque is independent of the particle size, which makes this technique adaptive to microscale systems. Because the particles disperse throughout the fluid volume, this technique should provide effective mixing even in irregular cavities. Future work in this area will involve large-scale simulations, to investigate the structure and phase lags of the particle agglomerates that form in a vortex field.

ACKNOWLEDGMENTS

Sandia is a multiprogram laboratory operated by Sandia Corporation, a Lockheed-Martin Company, for the United States Department of Energy under Contract No. DE-AC04-94AL85000. This work was supported by the Office of Basic Energy Research, DOE.

APPENDIX: FORCE BETWEEN TWO DIPOLES

To compute the angular force between two dipoles in the self-consistent local field approximation, we follow Ref. [4] and consider the change in their magnetostatic energy as a function of their orientation α relative to the applied field. The energy of each dipole is $-\frac{1}{2}\mathbf{m}\cdot\mathbf{H}_0$, so the energy of the pair is $U=-\mathbf{m}\cdot\mathbf{H}_0$. For particles of radius a the angular force is then just $F_\alpha=-(1/2a)\partial U/\partial\alpha$. All that is needed is an expression for the dipole moment of the particles as a function of their orientation.

For particles whose line of centers is at an angle α relative to the applied field $\mathbf{H}_0=H_0\hat{\mathbf{z}}$, it is useful to break the applied field into components parallel and perpendicular to the line of centers,

$$\mathbf{H}_\parallel = H_0(\cos\alpha\sin\alpha\,\hat{\mathbf{x}}+\cos^2\alpha\,\hat{\mathbf{z}}),$$

$$\mathbf{H}_\perp = H_0(-\cos\alpha\sin\alpha\,\hat{\mathbf{x}}+\sin^2\alpha\,\hat{\mathbf{z}}). \tag{A1}$$

For a field parallel to the line of centers the local field is $\mathbf{H}_{\rm loc}=\mathbf{H}_\parallel+2\mathbf{m}_\parallel/4\pi(2a)^3$, where the dipole moment $\mathbf{m}_\parallel=4\pi a^3\beta\mathbf{H}_{\rm loc}$. The local field is parallel to the applied field by symmetry, so combining these relations gives $\mathbf{H}_{\rm loc}=\mathbf{H}_\parallel/(1-\beta/4)$. This gives a dipole moment

$$\mathbf{m}_\parallel = \frac{4\pi a^3\beta H_0}{1-\beta/4}(\cos\alpha\sin\alpha\,\hat{\mathbf{x}}+\cos^2\alpha\,\hat{\mathbf{z}}). \tag{A2}$$

For a field perpendicular to the line of centers, the local field is $\mathbf{H}_{\rm loc}=\mathbf{H}_\perp-\mathbf{m}_\perp/4\pi(2a)^3$. The local field is again parallel to the applied field by symmetry, so combining these relations gives $\mathbf{H}_{\rm loc}=\mathbf{H}_\perp/(1+\beta/8)$. The dipole moment is thus

$$\mathbf{m}_\perp = \frac{4\pi a^3\beta H_0}{1+\beta/8}(-\cos\alpha\sin\alpha\,\hat{\mathbf{x}}+\sin^2\alpha\,\hat{\mathbf{z}}). \tag{A3}$$

The total dipole moment is $\mathbf{m}=\mathbf{m}_\parallel+\mathbf{m}_\perp$, and the energy of the pair is

$$U=-4\pi a^3\beta H_0^2\left(\frac{\cos^2\alpha}{1-\beta/4}+\frac{\sin^2\alpha}{1+\beta/8}\right). \tag{A4}$$

Differentiating with respect to α then gives the force

$$F_\alpha=-\frac{3\pi a^2\beta^2H_0^2}{4(1-\beta/4)(1+\beta/8)}\sin 2\alpha, \tag{A5}$$

which appears in Eq. (35).

[1] J. E. Martin, R. A. Anderson, and R. L. Williamson, J. Chem. Phys. **118**, 1557 (2003).
[2] J. E. Martin, E. Venturini, G. L. Gulley, and J. Williamson, Phys. Rev. E **69**, 021508 (2004).
[3] J. E. Martin, L. Shea-Rohwer, and K. Solis (unpublished).
[4] J. E. Martin and R. A. Anderson, J. Chem. Phys. **104**, 4814 (1996).
[5] S. Melle and J. E. Martin, J. Chem. Phys. **118**, 9875 (2003).
[6] O. Volkova, S. Cutillas, P. Carletto, G. Bossis, A. Cebers, and A. Meunier, J. Magn. Magn. Mater. **201**, 66 (1999).
[7] J. E. Martin, Phys. Rev. E **63**, 011406 (2000).
[8] O. Volkova, G. Bossis, P. Carletto, and A. Cebers, Int. J. Mod. Phys. B **15**, 878 (2001).
[9] S. Henley and F. E. Filisko, Int. J. Mod. Phys. B **16**, 2286

(2002).
[10] K. von Pfeil, M. D. Graham, D. J. Klingenberg, and J. F. Morris, J. Appl. Phys. **93**, 5769 (2003).
[11] T. C. Halsey, R. A. Anderson, and J. E. Martin, Int. J. Mod. Phys. B **10**, 3019 (1996); J. E. Martin, R. A. Anderson, and C. P. Tigges, J. Chem. Phys. **108**, 7887 (1998).
[12] J. R. Reitz and F. J. Milford, *Foundations of Electromagnetic Theory* (Addison-Wesley, Reading, MA, 1967).